Original Paper

European Neurology

Eur Neurol 2007;58:152–158
DOI: 10.1159/000104716

Received: September 6, 2006
Accepted: February 26, 2007
Published online: June 29, 2007

Autoantibodies against Glutamate Receptor ε_2-Subunit Detected in a Subgroup of Patients with Reversible Autoimmune Limbic Encephalitis

A. Kimura[a] T. Sakurai[a] Y. Suzuki[a] Y. Hayashi[a] I. Hozumi[a] O. Watanabe[b]
K. Arimura[b] Y. Takahashi[c] T. Inuzuka[a]

[a]Department of Neurology and Geriatrics, Gifu University Graduate School of Medicine, Gifu, [b]Department of Neurology and Geriatrics, Kagoshima University Graduate School of Medical and Dental Sciences, Kagoshima, and [c]National Epilepsy Center, Shizuoka Institute of Epilepsy and Neurological Disorders, Shizuoka, Japan

Key Words
Autoantibody · Glutamate receptor ε_2-subunit · Immunotherapy · Limbic encephalitis · N-methyl-D-aspartate glutamate receptor · Paraneoplastic syndrome

Abstract
We investigated the presence of autoantibodies against glutamate receptor (GluR) ε_2 in serum and cerebrospinal fluid (CSF) samples from 12 consecutive patients with acute encephalitis/encephalopathy by immunoblotting using recombinant GluRε_2 as antigen. In 4 patients, IgM autoantibodies against GluRε_2 were detected in CSF in the early phase of the disease but were not detectable after several months. Seizures and psychiatric symptoms were noted during the acute phase of the disease in these 4 patients, who showed various degrees of residual amnesia. Immunotherapy was performed on 3 patients (patients 1, 3 and 4), and they showed marked improvements. Immunohistochemistry using these patients' sera showed that immunoreactivity is specifically detected in the cytoplasm of rat hippocampal and cortical neurons. The clinical features and neuroimaging findings of patients with IgM autoantibodies against GluRε_2 in CSF resemble those of patients with reversible autoimmune limbic encephalitis.

Introduction

There are some reports that indicate the production of autoantibodies in patients with encephalitis [1–3] and encephalopathy [4]. Recently, autoantibodies against the N-methyl-D-aspartate (NMDA)-type glutamate receptor (GluR) ε_2 have been detected in patients with epilepsia partialis continua (EPC) causally related to Rasmussen syndrome [5], nonparaneoplastic limbic encephalitis [6] and acute encephalitis [5, 7]. The NMDA receptor, which is one of the three major ionotropic GluRs, is a heterodimer composed of ε- and ζ-subunit families [8]. There are 4 members in the ε-subunit family (ε_1–ε_4) [9]. The NMDA receptor channel is unique in terms of its functional properties [10, 11]. After birth, the expression of GluRε_2 mRNA becomes restricted to the forebrain, which includes the cerebral cortex and limbic system [12]. GluRε_2 is associated with memory and learning [10, 11]. Therefore, we investigated autoantibodies against GluRε_2 in serum and cerebrospinal fluid (CSF) samples from patients with acute encephalitis/encephalopathy to clarify its clinical features and immunological aspects.

Materials and Methods

We obtained serum and CSF samples from 12 consecutive patients with acute encephalitis/encephalopathy in our department from August 2003 to January 2005 (n = 12; male:female = 6:6; age

KARGER
Fax +41 61 306 12 34
E-Mail karger@karger.ch
www.karger.com

0014–3022/07/0583–0152$23.50/0

Accessible online at:
www.karger.com/ene

Dr. Akio Kimura
Department of Neurology and Geriatrics
Gifu University Graduate School of Medicine
1-1 Yanagido, Gifu City, Gifu 501-1194 (Japan)
Tel. +81 58 230 6253, Fax +81 58 230 6256, E-Mail kimura1@cc.gifu-u.ac.jp

Table 1. Autoantibodies against GluRε_2

Patient	Age/sex	Clinical diagnosis	Anti-GluRε_2 antibody	
			CSF IgM/IgG	serum IgM/IgG
1	45/F	ILE	+/+	+/+
2	62/M	ILE	+/+	–/–
3	53/F	ILE	+/+	+/+
4	30/M	ILE	+/–	+/+
5	22/F	ILE	–/–	–/–
6	68/M	bacterial meningoencephalitis	–/–	–/–
7	57/F	cryptococcal meningoencephalitis	–/–	–/–
8	18/F	MELAS	–/–	–/–
9	59/F	neuro-Sweet disease	–/–	–/–
10	65/M	PLE (anti-Hu antibody-positive)	–/–	–/+
11	26/M	etiology-unknown meningoencephalitis	–/–	+/–
12	56/M	brainstem encephalitis	–/–	–/–

ILE = Idiopathic limbic encephalitis; MELAS = mitochondrial encephalopathy with lactic acidosis and stroke-like episodes; PLE = paraneoplastic limbic encephalitis.

range = 18–68; mean age = 47 years; idiopathic limbic encephalitis, 5; etiology-unknown meningoencephalitis, 1; anti-Hu-antibody-positive paraneoplastic limbic encephalitis, 1; bacterial meningoencephalitis, 1; mitochondrial encephalopathy with lactic acidosis and stroke-like episodes, 1; cryptococcal meningoencephalitis, 1; brainstem encephalitis, 1; neuro-Sweet disease, 1).

Detection of Autoantibodies against GluRε_2

The method used has previously been reported [5]. The supernatants of cell extracts from stable NIH3T3-transformant cell lines expressing full-length GluRε_2 were subjected to SDS-PAGE, and the separated proteins on the gels were transferred to nitrocellulose membranes. The membranes were reacted with diluted sera or CSF and stained with alkaline-phosphatase-labeled secondary antibodies (IgG or IgM; Jackson Immunoresearch, West Grove, Pa., USA). Anti-GluRε_2 autoantibodies were detected as a band corresponding to approximately 180 kDa.

Immunohistochemistry Using Patient's Serum

Under ether anesthesia, adult Sprague-Dawley rats were sacrificed. The cerebrums were immediately removed and frozen in dry-ice powder. Frozen sections (8 μm thick) of the cerebrums were fixed in 4% paraformaldehyde. The sections were incubated with serially diluted serum from a patient or with an anti-NMDAε_2 antibody (1:500; Santa Cruz Biotechnology, USA). Then, the sections were incubated with a goat biotinylated anti-human IgM (μ-chain-specific) antibody (Vector, USA) or a rabbit biotinylated anti-goat IgG (H+L) antibody (Chemicon, USA). After washing, the sections were reacted with a streptavidin-peroxidase complex (Nichirei, Japan). The reactions were finally developed with 3,3′-diaminobenzidine tetrahydrochloride (Wako, Japan) and 0.01% H_2O_2 in PBS. For adsorption tests, frozen sections after blocking were immunostained with a patient's serum (1:2,000) or with the anti-NMDAε_2 antibody (1:500) that was incubated for 24 h with extracts from transformant cells expressing full-length GluRε_2.

Results

Detection of Autoantibodies against GluRε_2

The IgM autoantibody against GluRε_2 in CSF was detected in 4 out of 12 consecutive patients in the early phase of the disease but was not detectable after several months (table 1). The IgG autoantibody against GluRε_2 in CSF was detected in 3 of these 4 patients (patients 1–3). No autoantibodies against GluRε_2 were detected in the CSF of the other patients. In the early phase of the disease, patients 1 and 4 had IgM and IgG autoantibodies against GluRε_2 in their serum. Patient 3 had only the IgM autoantibody but became positive for the IgG autoantibody 2 months later.

Clinical Features

All the patients who had the IgM autoantibody against GluRε_2 in CSF presented with seizures (i.e. partial seizures evolving to secondary generalized seizures) and psychiatric symptoms (i.e. hallucination, behavioral changes and agitation) in the early phase of the disease and developed prolonged consciousness disturbances with status epilepticus (table 2). None of these patients presented with paralysis or disturbances in sensation in the chronic stage. However, all of them presented with various degrees of recent memory disturbance and amnesia. Patient 3 showed residual psychiatric symptoms after treatment. Three patients (patients 1, 3 and 4) received intravenous methylprednisolone pulse therapy and showed improvement in their seizures and consciousness levels.

Table 2. Clinical features of patients with IgM autoantibody against GluRε_2 in CSF

Patient	Age/sex	Clinical diagnosis	Initial symptoms	Sequelae	Steroid treatment
1	45/F	ILE	convulsion, visual and olfactory hallucinations	disorientation, amnesia, recent memory disturbance	responsive
2	62/M	ILE	convulsion, auditory hallucination	disorientation, amnesia, recent memory disturbance	not performed
3	53/F	ILE	convulsion, behavioral changes	disorientation, amnesia, recent memory disturbance, psychiatric symptoms	responsive
4	30/M	ILE	convulsion, behavioral changes	amnesia, recent memory disturbance	responsive

ILE = Idiopathic limbic encephalitis.

Case Presentation

Here, we describe a representative patient with IgM autoantibodies against GluRε_2 in CSF. Patient 1 has been described previously [6].

Patient 4 was a 30-year-old male initially complaining of headaches with fever. Throughout 1 week, he showed no improvement in these symptoms and presented with agitation and behavioral disturbance. He was admitted to a nearby hospital because he suddenly suffered a generalized tonic seizure. After admission to the hospital, he was treated with antiepileptic drugs and intravenous acyclovir. However, he developed consciousness disturbance and status epilepticus. Then, he was transferred to our hospital. He had an unremarkable medical history, a temperature of 37.7°C, a pulse of 74/min and a blood pressure of 105/68 mm Hg. On neurological examination, he exhibited somnolence. There was lateral gaze-evoked nystagmus. The deep tendon reflexes of all four limbs were slightly hypoactive. There were no pathological reflexes. No meningeal signs were observed. After his consciousness level had improved, muscle strength, sensation and coordination became normal. Laboratory tests revealed leukocytosis and elevated levels of myogenic enzymes: white blood cell count, 13.8 × $10^3/\mu l$; creatine kinase level, 3,285 IU/l; aspartate aminotransferase level, 80 IU/l, and lactate dehydrogenase level, 394 IU/l. The serum C-reactive protein level was slightly elevated to 1.89 mg/dl. The serum antinuclear antibody was absent. IgM and IgG autoantibodies against GluRε_2 were present in serum on the day of admission. Analysis of CSF showed 34 cells/mm^3 (mononuclear cells only), 36 mg/dl total protein and 68 mg/dl glucose. He had a mildly elevated IgG index (0.73). IgM and IgG antibodies against herpes simplex virus, cytomegalovirus and varicella-zoster virus were absent in paired sera and CSF tested at 2-week intervals. PCR analysis showed negativity for herpes simplex virus, cytomegalovirus and human herpesvirus 6/7 DNA in CSF. The IgM autoantibody against GluRε_2 was present, but the IgG autoantibody was absent in CSF on the day of admission. EEG revealed diffuse θ-waves with small spikes in the left temporal lobe. Brain MRI revealed no abnormal intensity changes but diffuse cortical edema. ^{99m}Tc-ECD SPECT performed on the 14th day of hospitalization revealed hypoperfusion in the diffuse cerebral cortex and bilateral mesial temporal lobes. After admission, he was treated with phenytoin. However, the seizures were difficult to control and required treatment with anesthetic agents (pentobarbital sodium and midazolam) under respiratory management. He was treated with an intravenous infusion of 1 g of methylprednisolone for 3 consecutive days. He showed improvement in consciousness level and the frequency of the convulsions decreased following the treatment. However, approximately 2 weeks after steroid therapy, his seizures increased in frequency again, and intravenous immunoglobulin (400 mg/kg/day for 5 consecutive days) was administered. His condition slowly improved. On the 36th day of hospitalization, he required no respiratory management. Afterwards, we carried out the administration of intravenous immunoglobulin and steroid pulse therapy, and his seizures disappeared completely. However, he showed disorientation and severe amnesia. Revised Hasegawa Dementia Scale (HDS-R) and Mini Mental State Examination scores determined approximately 3 months after admission were 10/30 and 13/30, respectively. His Revised Wechsler Adult Intelligence Scale (WAIS-R) full-scale IQ was less than 40, and his verbal and performance subscale scores were 51 and less than 45, respectively. All Revised Wechsler Memory Scale (WMS-R) indexes showed significantly low scores (gen-

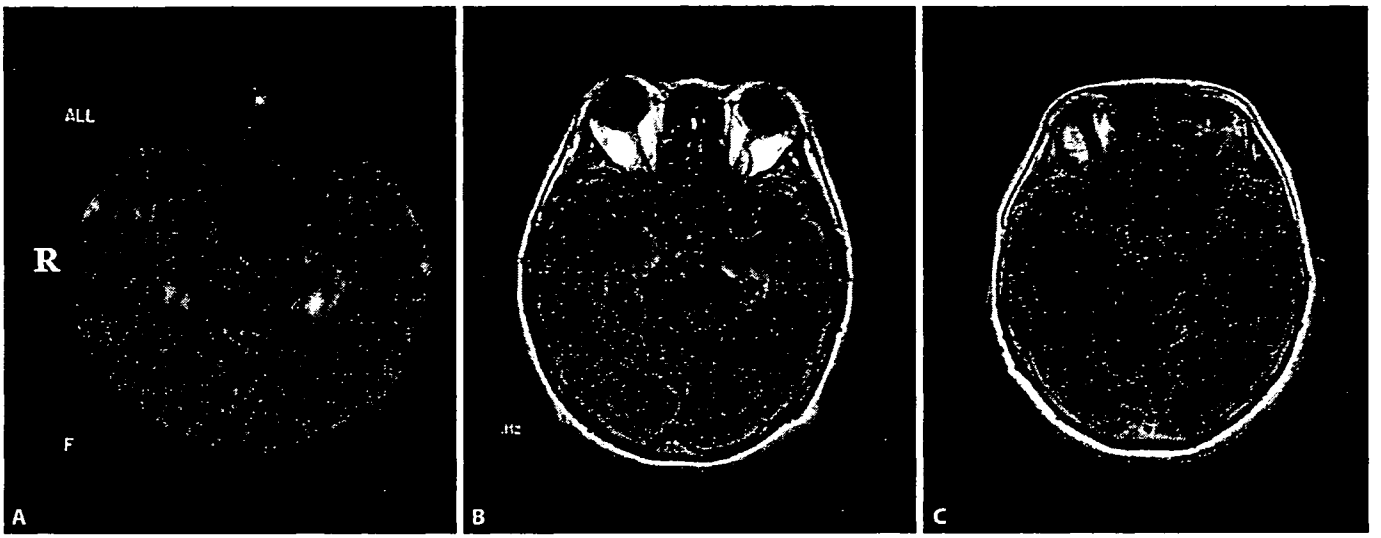

Fig. 1. MR images of patient 1. An axial diffusion-weighted image (**A**) and a fluid-attenuated inversion recovery image (**B**) show hyperintensity in the bilateral mesial temporal lobes in the acute phase (2 days after admission). **C** A follow-up T_1-weighted MR image shows the disappearance of signal abnormalities and the appearance of bilateral hippocampal and mild cortical atrophies (1 year after the disease onset).

Table 3. Laboratory and neuroimaging findings of patients with IgM autoantibody against GluRε_2 in CSF

Patient	WBC n/mm³	CRP mg/dl	CSF cell n/mm³	CSF protein mg/dl	IgG index	Other autoantibodies	Initial brain MRI
1	13,800	1.30	81 (M 81)	30	0.53	TPO Ab	hyperintensity in bilateral mesial temporal lobes
2	3,500	0.42	10 (M 9, P 1)	67	0.80	–	hyperintensity in left mesial temporal lobe
3	18,240	<0.05	7 (M 1, P 6)	38	n.e.	ANA	hyperintensity in bilateral mesial temporal lobes, insulae and cingulate gyri
4	17,090	1.89	34 (M 34)	36	0.73	–	normal

WBC = White blood cells; CRP = C-reactive protein; MRI comprised diffusion-weighted, T_2-weighted and fluid-attenuated inversion recovery imagings; ANA = antinuclear antibody; TPO Ab = thyroid peroxidase antibody; M = mononuclear cell; P = polynuclear cell; n.e. = not examined.

eral memory <50; verbal memory = 54; delayed memory <50; visual memory <50; attention and concentration <50). It was difficult for him to immediately recall things related to logical memory after hearing them. He showed no higher functional impairments such as aphasia, apraxia and agnosia. His memory and cognitive state slowly improved, and he was discharged 4 months after admission. Eight months after the disease onset, his memory and cognitive scale scores improved significantly [HDS-R score 25/30, WAIS-R IQ (total IQ, 70; verbal IQ, 63; performance IQ, 87), WMS-R scores (general memory, 53; verbal memory, 57; delayed memory, 60; visual memory, 70; attention and concentration, 61)]. Brain MRI revealed no intensity changes; however, mild cortical atrophy was observed 6 months after the disease onset.

Laboratory Findings

Virological examinations (table 3) showed negativity for IgM and IgG antibodies against the herpes simplex virus, cytomegalovirus and varicella-zoster virus in paired sera and CSF tested at 2-week intervals. PCR analysis showed negativity for the herpes simplex virus and human herpesvirus 6/7 DNA in CSF. Patient 3 had the antinuclear antibody (ELISA: 34.4, normal <20.0) in her se-

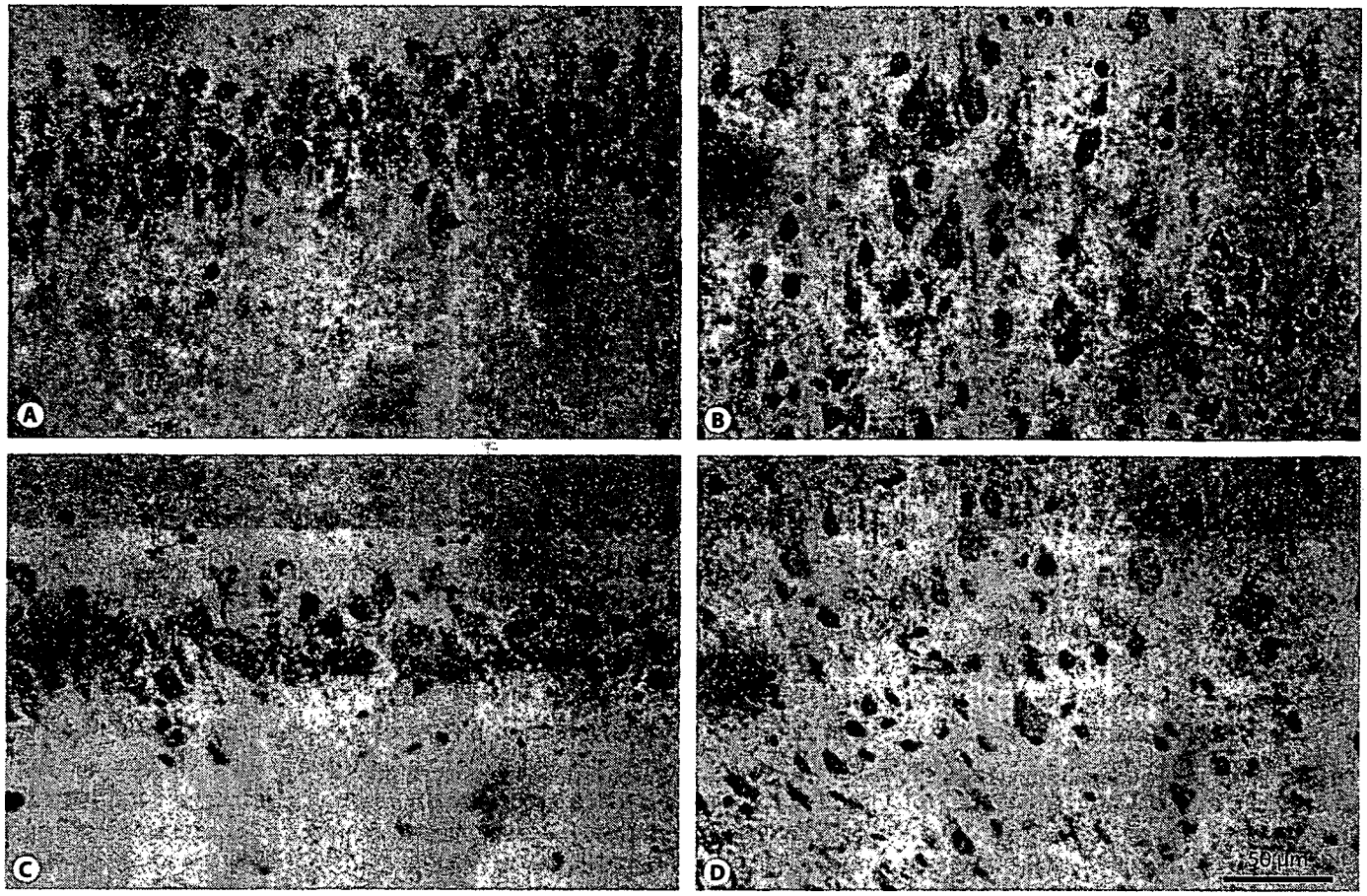

Fig. 2. Immunohistochemistry. **A**, **B** Coronal sections of rat brain immunoreacted with serum samples from patient 1. **C**, **D** Coronal sections immunoreacted with serum samples from patient 4. The diluted sera (1:2,000) of these patients reacted with the cytoplasm of rat hippocampal (**A**, **C**) and cortical (**B**, **D**) neurons. The same pattern of reactivity was observed for the serum samples from patient 3 and the anti-NMDAε_2 antibody. The sections are slightly counterstained with hematoxylin. Magnification ×400.

rum. Patient 1 showed an elevated level of the antithyroperoxidase antibody in the serum, which was not detected in CSF. We measured the titers of voltage-gated potassium channel (VGKC) antibodies by radioimmunoassay using whole rabbit brain homogenate as described previously [13]. The titers of VGKC antibodies showed normal levels in these 4 patients (patient 1: 0 pM, patient 2: 21 pM, patient 3: 0 pM, patient 4: 18 pM, normal range <100 pM).

Neuroimaging and Physiological Examination

Brain MRI at disease onset showed signal abnormalities in the bilateral mesial temporal lobes in patients 1 and 3 and on one side of the mesial temporal lobe in patient 2. In patient 4, brain MRI showed no signal abnormalities. However, several months (range, 6 months to 1 year) after the disease onset, cerebral atrophy of various degrees, including atrophy in the mesial temporal lobe, was common (fig. 1). SPECT was performed in the acute or subacute phase. All of the patients except patient 1 showed hypoperfusion in the mesial temporal lobe. In patient 1, ^{99m}Tc-HMPAO SPECT performed the day after admission revealed hyperperfusion in the bilateral mesial temporal lobes; however, hypoperfusion was observed 17 months later. All the patients showed irregular diffuse cortical hypoperfusion. In 3 patients, EEG revealed small focal spikes. In all the patients, a mixture of diffuse θ-waves was observed. No tumors were detected in any of the patients using various methods [chest, abdomen and pelvic CTs (all patients), whole-body FDG-PET (patient 1) and gallium scintigraphy (patient 2)].

Immunohistochemical Findings

The diluted serum samples from patients 1, 3 and 4 reacted with the cytoplasm of rat hippocampal and cerebral cortical neurons (fig. 2). The most appropriate dilution of serum for immunohistochemical staining was 1:2,000–4,000. The sections incubated with the anti-NMDAε_2 antibody showed the same pattern of immunoreactivity as those incubated with the patients' sera. The serum of the healthy control did not significantly immunoreact with the sections. The immunoreactivity of sera of the 3 above-mentioned patients to the anti-GluRε_2 antibody was markedly decreased by prior incubation with the supernatants of extracts from stable transformant cells expressing GluRε_2. Patients 1, 2 and 3 were negative for serum paraneoplastic anti-Yo, anti-Hu, anti-Ri, anti-CV2, anti-Tr, anti-Ma-2 and antiamphiphysin antibodies.

Discussion

We presented 4 patients with acute encephalitis who had IgM autoantibodies against GluRε_2 in CSF in the early phase of the disease; however, these antibodies were not detectable after several months. Other acute encephalitis/encephalopathy patients (patients 5–12) had neither the IgG nor IgM autoantibody against GluRε_2 in CSF. Four antibody-positive patients had the characteristic clinical features of reversible autoimmune limbic encephalitis such as intractable convulsion, psychiatric symptoms, recent memory disturbance and sufficient responsiveness to immunotherapy. Concerning the cause of limbic encephalitis, there are many reports in which limbic encephalitis is associated with cancer, most commonly a small-cell carcinoma of the lung [14–20]. The 4 antibody-positive patients had no findings of viral infection or cancer. Several reports have been published concerning the immunotherapy response form of nonparaneoplastic limbic encephalitis [21–26]. Recently, a VGKC antibody has been detected in patients with reversible autoimmune limbic encephalitis [27–32]. However, the titers of VGKC antibodies were normal in our 4 antibody-positive patients' sera. We speculate that reversible autoimmune limbic encephalitis is heterogeneous. Some forms of this disease may be mediated by autoantibodies against antigens such as ion channels or ionotropic receptors in the limbic system.

In our immunohistochemical analysis of the sera of patients with the IgM autoantibody against GluRε_2, immunoreactivity was detected in the cytoplasm of neurons in the hippocampus and cerebral cortex. The immunoreactivity was specifically demonstrated using an immunoadsorption test. The NMDA receptor is one of the ionotropic glutamate receptors essential for excitatory neurotransmission and synaptic plasticity, which underlie memory and learning [10, 11]. An antibody-mediated disturbance of NMDA-type GluR function might influence synaptic plasticity in the hippocampus and cortical neuronal excitability. The clinical response to immunotherapy and the results of immunoblotting and immunohistochemistry suggest that IgM autoantibodies may be related to pathogenesis in a subgroup of patients with reversible autoimmune limbic encephalitis.

In a previous study, autoantibodies against GluRε_2 were detected in patients with chronic EPC causally related to Rasmussen syndrome [7]. There are some reports that these antibodies have also been detected in patients with encephalitides other than chronic EPC [6, 7]. In this study, we detected autoantibodies against GluRε_2 in patients with reversible autoimmune limbic encephalitis. We suggest that autoantibodies against GluRε_2 contribute to the onset of localized encephalitides such as EPC and reversible autoimmune limbic encephalitis [7].

Acknowledgments

We wish to thank Dr. K. Tanaka of the Department of Neurology, Brain Research Institute, Niigata University, for evaluating serum paraneoplastic antibodies. This research was partially supported by a Grant-in-Aid for Young Scientists (B 1690486) from the Japanese Ministry of Education, Culture, Sports, Science and Technology, a Grant-in-Aid for Scientific Research (No. 17591133) and a Health and Labour Sciences Research Grant for Research on Psychiatry and Neurological Diseases and Mental Health (H17-017).

References

1 Dale RC, Church AJ, Surtees RA, Lees AJ, Adcock JE, Harding B, Neville BG, Giovannoni G: Encephalitis lethargica syndrome: 20 new cases and evidence of basal ganglia autoimmunity. Brain 2004;127:21–33.

2 Rogers SW, Andrews PI, Gahring LC, Whisenand T, Cauley K, Crain B, Hughes TE, Heinemann SF, McNamara JO: Autoantibodies to glutamate receptor GluR3 in Rasmussen's encephalitis. Science 1994;265:648–651.

3 Watson R, Jepson JE, Bermudez I, Alexander S, Hart Y, McKnight K, Roubertie A, Fecto F, Valmier J, Sattelle DB, Beeson D, Vincent A, Lang B: α_7-Acetylcholine receptor antibodies in two patients with Rasmussen encephalitis. Neurology 2005;65:1802–1804.

4 DeGiorgio LA, Konstantinov KN, Lee SC, Hardin JA, Volpe BT, Diamond B: A subset of lupus anti-DNA antibodies cross-reacts with the NR2 glutamate receptor in systemic lupus erythematosus. Nat Med 2001;7:1189–1193.
5 Takahashi Y, Mori H, Mishina M, Watanabe M, Fujiwara T, Shimomura J, Aiba H, Miyajima T, Saito Y, Nezu A, Nishida H, Imai K, Sakaguchi N, Kondo N: Autoantibodies to NMDA receptor in patients with chronic forms of epilepsia partialis continua. Neurology 2003;61:891–896.
6 Hayashi Y, Matsuyama Z, Takahashi Y, Wakida K, Hashizume T, Kimura A, Hozumi I, Murase M, Inuzuka T: A case of non-herpetic acute encephalitis with autoantibodies for ionotropic glutamate receptor δ_2 and ε_2 (in Japanese). Rinsho Shinkeigaku 2005;45:657–662.
7 Takahashi Y: Infections as causative factors of epilepsy. Future Neurol 2006;1:291–302.
8 Kutsuwada T, Kashiwabuchi N, Mori H, Sakimura K, Kushiya E, Araki K, Meguro H, Masaki H, Kumanishi T, Arakawa M, Mishina M: Molecular diversity of the NMDA receptor channel. Nature 1992;358:36–41.
9 Mori H, Mishina M: Structure and function of the NMDA receptor channel. Neuropharmacology 1995;34:1219–1237.
10 Kutsuwada T, Sakimura K, Manabe T, Takayama C, Katakura N, Kushiya E, Natsume R, Watanabe M, Inoue Y, Yagi T, Aizawa S, Arakawa M, Takahashi T, Nakamura Y, Mori H, Mishina M: Impairment of suckling response, trigeminal neuronal pattern formation and hippocampal LTD in NMDA receptor ε_2 subunit mutant mice. Neuron 1996;16:333–344.
11 Tang Y, Shimizu E, Dube GR, Rampon C, Kerchner GA, Zhuo M, Liu G, Tsien JZ: Genetic enhancement of learning and memory in mice. Nature 1999;401:63–69.
12 Watanabe M, Inoue Y, Sakimura K, Mishina M: Developmental changes in distribution of the NMDA receptor channel subunit mRNAs in the brain. Neuroreport 1992;3:1138–1140.
13 Shillito P, Molenaar PC, Vincent A, Leys K, Zheng W, van den Berg RJ, Plomp JJ, Van Kempen GTH, Chauplannaz G, Wintzen AR, van Dijk JG, Newsom-Davis J: Acquired neuromyotonia: evidence for autoantibodies directed against K^+ channels of peripheral nerves. Ann Neurol 1995;38:714–722.
14 Gultekin SH, Rosenfeld MR, Voltz R, Eichen J, Posner JB, Dalmau J: Paraneoplastic limbic encephalitis: neurological symptoms, immunological findings and tumour association in 50 patients. Brain 2000;123:1481–1494.
15 Voltz R. Paraneoplastic neurological syndromes: an update on diagnosis, pathogenesis, and therapy. Lancet Neurol 2002;1:294–305.
16 Kinirons P, Fulton A, Keoghan M, Brennan P, Farrell MA, Moroney JT: Paraneoplastic limbic encephalitis (PLE) and chorea associated with CRMP-5 neuronal antibody. Neurology 2003;61:1623–1624.
17 Pittock SJ, Lucchinetti CF, Parisi JE, Benarroch EE, Mokri B, Stephan CL, Kim KK, Kilimann MW, Lennon VA: Amphiphysin autoimmunity: paraneoplastic accompaniments. Ann Neurol 2005;58:96–107.
18 Dalmau J, Graus F, Villarejo A, Posner JB, Blumenthal D, Thiessen B, Saiz A, Meneses P, Rosenfeld MR: Clinical analysis of anti-Ma2-associated encephalitis. Brain 2004;127:1831–1844.
19 Alamowitch S, Graus F, Uchuya M, Rene R, Bescansa E, Delattre JY: Limbic encephalitis and small cell lung cancer: clinical and immunological features. Brain 1997;120:923–928.
20 Inuzuka T: Limbic encephalitis: etiology, pathogenesis, diagnosis and therapy (in Japanese). Rinsho Shinkeigaku 2004;44:799–801.
21 Kusuhara T, Shoji H, Kaji M, Ayabe M, Hino H: Non-herpetic acute limbic encephalitis (in Japanese). Rinsho Shinkeigaku 1994;34:1083–1088.
22 Bien CG, Schulze-Bonhage A, Deckert M, Urbach H, Helmstaedter C, Grunwald T, Schaller C, Elger CE: Limbic encephalitis not associated with neoplasm as a cause of temporal lobe epilepsy. Neurology 2000;55:1823–1828.
23 Asaoka K, Shoji H, Nishizaka S, Ayabe M, Abe T, Ohori N, Ichiyama T, Eizuru Y: Non-herpetic acute limbic encephalitis: cerebrospinal fluid cytokines and magnetic resonance imaging findings. Intern Med 2004;43:42–48.
24 Watanabe Y, Shimizu Y, Ooi S, Tanaka K, Inuzuka T, Nakashima K: Steroid-responsive limbic encephalitis. Intern Med 2003;42:428–432.
25 Ances BM, Vitaliani R, Taylor RA, Liebeskind DS, Voloschin A, Houghton DJ, Galetta SL, Dichter M, Alavi A, Rosenfeld MR, Dalmau J: Treatment-responsive limbic encephalitis identified by neuropil antibodies: MRI and PET correlates. Brain 2005;128:1764–1777.
26 Mori M, Kuwabara S, Yoshiyama M, Kanesaka T, Ogata T, Hattori T: Successful immune treatment for non-paraneoplastic limbic encephalitis. J Neurol Sci 2002;201:85–88.
27 Buckley C, Oger J, Clover L, Tuzun E, Carpenter K, Jackson M, Vincent A: Potassium channel antibodies in two patients with reversible limbic encephalitis. Ann Neurol 2001;50:73–78.
28 Thieben MJ, Lennon VA, Boeve BF, Aksamit AJ, Keegan M, Vernino S: Potentially reversible autoimmune limbic encephalitis with neuronal potassium channel antibody. Neurology 2004;62:1177–1182.
29 Vincent A, Buckley C, Schott JM, Baker I, Dewar BK, Detert N, Clover L, Parkinson A, Bien CG, Omer S, Lang B, Rossor MN, Palace J: Potassium channel antibody-associated encephalopathy: a potentially immunotherapy-responsive form of limbic encephalitis. Brain 2004;127:701–712.
30 Fauser S, Talazko J, Wagner K, Ziyeh S, Jarius S, Vincent A, Schulze-Bonhage A: FDG-PET and MRI in potassium channel antibody-associated non-paraneoplastic limbic encephalitis: correlation with clinical course and neuropsychology. Acta Neurol Scand 2005;111:338–343.
31 Pozo-Rosich P, Clover L, Saiz A, Vincent A, Graus F: Voltage-gated potassium channel antibodies in limbic encephalitis. Ann Neurol 2003;54:530–533.
32 Vincent A, Bien CG: Temporal lobe seizures, amnesia and autoantibodies – Identifying a potentially reversible form of non-paraneoplastic limbic encephalitis. Epileptic Disord 2005;7:177–179.

Original Paper

Pathobiology

Pathobiology 2007;74:169–176
DOI: 10.1159/000103376

Received: October 23, 2006
Accepted after revision: February 21, 2007

Expression of Autophagy-Associated Genes in Skeletal Muscle: An Experimental Model of Chloroquine-Induced Myopathy

Noriyuki Kimura Toshihide Kumamoto Yosuke Kawamura Takahiro Himeno
Ken-ichro Nakamura Hidetsugu Ueyama Ryuki Arakawa

Department of Neurology and Neuromuscular Disorders, Faculty of Medicine, Oita University, Oita, Japan

Key Words
Apg12 · Apg5 · Autophagy · Chloroquine · GNE · LC3 · Lysosome · mRNA · Rimmed vacuoles

Abstract
Objective: Chloroquine modulates autophagocytic protein degradation in the lysosome system, thereby inducing the formation of rimmed vacuoles consisting of autophagosomes and autolysosomes in skeletal muscle. The goal of this study was to investigate the contribution of the lysosomal system, particularly autophagosome formation (an autophagic process) at the molecular level, to the abnormal accumulation of vacuoles in an experimental model of chloroquine-induced myopathy. ***Methods:*** Histological, immunohistochemical and semiquantitative reverse transcriptase-polymerase chain reaction studies were performed on innervated and denervated rat soleus muscles after treatment with either saline or chloroquine. ***Results:*** Accumulation of rimmed vacuoles was observed only in chloroquine-treated denervated muscles. Microtubule-associated protein-1 light chain-3 (LC3) protein and mRNA levels were significantly increased exclusively in denervated muscles from chloroquine-treated rats, whereas Apg5 and Apg12 mRNA levels did not change significantly. Further, the mRNA levels of UDP-N-acetylglucosamine 2-epimerase/N-acetylmannosamine kinase (GNE), which are associated with distal myopathy with rimmed vacuoles showing numerous rimmed vacuoles in its skeletal muscle, were not decreased in denervated muscles treated with chloroquine. ***Conclusions:*** LC3 mRNA may increase in association with rimmed vacuole formation in denervated muscles from chloroquine-treated rats, suggesting an increase in autophagy at the molecular level. Abnormal accumulation of rimmed vacuoles in this myopathy does not appear to be mediated by inhibition of autophagosome-related genes or GNE gene.

Introduction

Chloroquine, a lysosomotrophic agent, modulates autophagic protein degradation in the lysosome system, thereby inducing the formation of rimmed vacuoles consisting of dense granular bodies and vacuoles including many variably sized and shaped autophagosomes in skeletal muscles [1–3]. We previously demonstrated an increased number of rimmed vacuoles in denervated chloroquine-treated rat muscle but not in innervated chloroquine-treated muscle or in innervated or denervated muscles of saline-treated rats [2]. Interestingly, while vacuoles were only increased in chloroquine-treated denervated muscles, there was no difference in lysosomal enzyme activity when comparing saline-treated and chlo-

KARGER
Fax +41 61 306 12 34
E-Mail karger@karger.ch
www.karger.com

1015–2008/07/0743–0169$23.50/0

Accessible online at:
www.karger.com/pat

Dr. Toshihide Kumamoto
Department of Neurology and Neuromuscular Disorders
Faculty of Medicine, Oita University, Idaigaoka 1-1, Hasama, Yufu
Oita 879-5593 (Japan)
Tel. +81 97 586 5814, Fax +81 97 586 6502, E-Mail kumagoro@med.oita-u.ac.jp

roquine-treated denervated muscles. Since an autophagic-lysosome process mediates degradation of muscle fibers in denervated muscles [2], chloroquine-induced dysfunction of the autophagic-lysosome process could represent an excellent mechanistic explanation for vacuole formation.

The autophagic-lysosome system plays an important role in the degradation and turnover of intracellular proteins, lipids, glycogens and organelles in skeletal muscle [4, 5]. While this pathway has been well characterized, it is not clear how chloroquine treatment affects this process. Furthermore, the pathomechanism of abnormal rimmed vacuole accumulation in those muscles remains unknown.

Recent studies have reported that Apg12, Apg5 and microtubule-associated protein-1 light chain-3 (LC3) are involved in the process of autophagy [6, 7]. Indeed, autophagy-defective mutations (apg ant mut) in Apg12 and Apg5 result in abnormalities in autophagosome formation. Further, the Apg12p-conjugated Apg5p complex is essential for formation of the autophagosome precursor and final product [6, 7]. This conjugation is found in various mammalian tissues, including skeletal muscle, and is thought to function in autophagy in the mammalian cell [6]. However, there is no direct evidence that the system is related to autophagy in rat skeletal muscle. In fact, the expression of the Apg12-conjugated Apg5 complex has only rarely been studied in skeletal muscle, especially under pathologic conditions.

Another ubiquitin-like modification, LC3, is also essential for the formation of the autophagosome [8–11]. LC3, a homologue of Apg8p/Aut7p in yeast, is associated with the autophagosome membrane after processing and plays a critical role in the formation of autophagosomes [12]. LC3 is present in various mammalian cells, including myocytes, as well as in yeast. Two forms of LC3, LC3-1 and -II, are produced posttranslationally in various cells. LC3-1 occurs in the cytoplasm, while LC3-II occurs in the autophagosome membrane. The amount of LC3-II correlated with the extent of autophagosome formation. LC3-II is the first identified mammalian protein to specifically associate with autophagosome membranes [13].

Rimmed vacuoles are frequently observed in the skeletal muscles of patients with distal myopathy with rimmed vacuoles, and UDP-N-acetylglucosamine 2-epimerase/N-acetylmannosamine kinase (GNE) gene mutations have been detected in this myopathy [14, 15]. However, it is not clear whether or not chloroquine modulates GNE gene expression in skeletal muscle.

Therefore, the goal of this study was to investigate the contribution of the lysosomal system, particularly autophagosome formation (an autophagic process), and GNE expression to the abnormal accumulation of vacuoles in an experimental model of chloroquine-induced myopathy.

Materials and Methods

Animals

The left hind legs of 30 adult male Wistar rats (200–250 g) were denervated by ligation of the sciatic nerve, as previously described [2]. Chloroquine chloride (50 mg/kg body weight) was injected intraperitoneally into 15 rats twice daily, beginning the day after denervation. The remaining 15 rats received injection of saline. The soleus muscles from the right (innervated) and left (denervated) legs were obtained from chloroquine- and saline-treated rats on days 2, 4 and 8 after the initial injection. The muscles were then rapidly frozen in isopentane cooled in liquid nitrogen.

Histologic and Immunohistochemical Studies

Routine histologic analysis was performed using cryostat sections (10-μm thick), as described previously [2]. Hematoxylin-eosin preparations of each specimen were analyzed with a Nikon Cosmozon ISA image apparatus (Nikon, Tokyo, Japan) attached to a Macintosh computer (Apple Computer, Cupertino, Calif., USA). The number of fibers with dense granular bodies or vacuoles at the light-microscopic level was determined in 400 muscle fibers per muscle.

For immunofluorescence analysis, the sections were incubated at room temperature for 2 h with a polyclonal goat antibody against the LC3 (diluted 1:50; Santa Cruz Biotechnology, Santa Cruz, Calif., USA), then with Texas red-labeled horse anti-goat IgG (diluted 1:100; Vector Laboratories, Burlingame, Calif., USA) for 1 h, rinsed, and mounted on slides for visualization by fluorescence microscopy. Images were captured using a Carl Zeiss LSM5 Pascal-V3.2 confocal microscopy system (Carl Zeiss, Jena, Germany).

Immunostaining was specific because there was no staining when sections were allowed to react without the first-layer antibodies or when normal goat serum was substituted for the antibody.

Semiquantitative Reverse Transcriptase Polymerase Chain Reaction (RT-PCR)

Innervated and denervated soleus muscles from saline- and chloroquine-treated rats that had been histologically examined were excised and frozen rapidly in liquid nitrogen. Total RNA was isolated from the specimens with acid guanidinium thiocyanate buffer (Nippon Gene, Tokyo, Japan) according to the manufacturer's instructions. Complementary DNA (cDNA) was synthesized from 1 μg of total RNA using 200 units of Moloney murine leukemia virus reverse transcriptase (Gibco, Gaithersburg, Md., USA) and 1 μg of oligo-(dT) 12–18 primer (Invitrogen, Carlsbad, Calif., USA).

PCR primers were constructed on the basis of published nucleotide sequences of the rat LC3 gene [16] (5′-CA GGA TCC

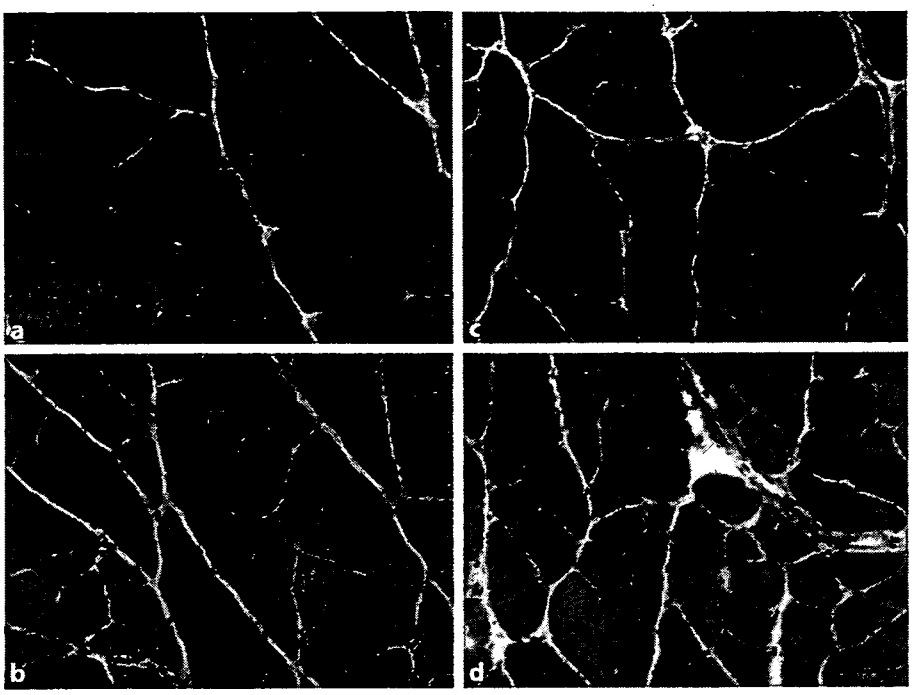

Fig. 1. Cross-sections of rat soleus muscles after 8 days of saline or chloroquine treatment. A large number of dense granular bodies and vacuoles are present in the denervated muscles from chloroquine-treated rats (**d**) but are absent in innervated muscles from chloroquine-treated rats (**c**) and in innervated (**a**) and denervated (**b**) muscles from saline-treated rats. HE. Bar = 50 μm.

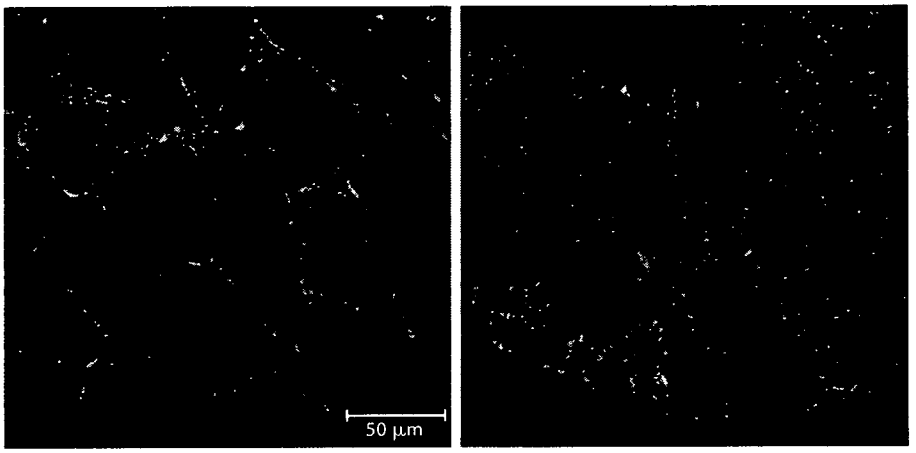

Fig. 2. Immunofluorescence staining for anti-LC3 antibody in innervated and denervated soleus muscles after 8 days of saline or chloroquine treatment. Immunoreactivity for LC3 was increased in the denervated muscles from chloroquine-treated rats (**b**) compared to the innervated saline-treated muscles (**a**). Bar = 50 μm.

ATG CCG TCC CAG AAG ACC-3′, sense; 5′-GTC CCT TTT TGC CTT GGT AG-3′ antisense), the mouse Apg5 gene [7] (5′-GCT TCG AGA TGT GTG GTT-3′, sense; 5′-AAT GTA CTG TGA TGT TCC-3′, antisense), the mouse Apg12 gene [7] (5′-CCG GAG ACA CCA AGA AAA-3′, sense; 5′-AGG GGC AAA GGA CTG ATT-3′, antisense), the rat GNE gene [17] (5′-TGG TGG TGC TGG GCT CTC-3′, sense; 5′-TGC TTA ATG TCG GTG GTC-3′, antisense), and the rat glycerol aldehyde 3-phosphate dehydrogenase (GAPDH) gene [18] (5′-GCC AAG TTC AAT GGC ACA GT-3′, sense; 5′- AAG GTG GAG GAA TGG GAG TT-3′, antisense). The PCR reactions were performed in a final volume of 50 μl in a DNA thermal cycler (Astec, Tokyo, Japan). Each PCR reaction mixture contained 1 μl of cDNA, 10× PCR buffer (200 mM Tris-HCl, pH 8.4, and 500 mM KCl), 2.5 mM dNTP, 25 mM $MgCl_2$, 0.5 μM of each set of primers, and 2.5 units of Taq DNA polymerase (Gibco). The PCR mixture was incubated at 94°C for 2 or 3 min, followed by 28 or 35 cycles of amplification. Each cycle consisted of 30 s of denaturation at 94°C, 30 s of annealing at 58 or 60°C, and 30 s or 1 min of extension at 72°C. After 28 or 35 cycles, a final extension step at 72°C for 3 min was performed. A negative control consisted of a reaction without inclusion of the reverse transcriptase. Efficiency of reverse transcription was controlled by PCR using GAPDH-specific primers. Target sequences of these primers were located on different exons. Only a proper reverse transcriptase reaction resulted in an amplification of a PCR product of the correct fragment size. After 2% agarose gel electrophoresis, scanning densitometry (Epson GT-8000 scanner; Epson, Tokyo, Japan) was used to determine the peak areas and assess the relative amounts of mRNA in ethidium bromide-stained bands. The intensity of

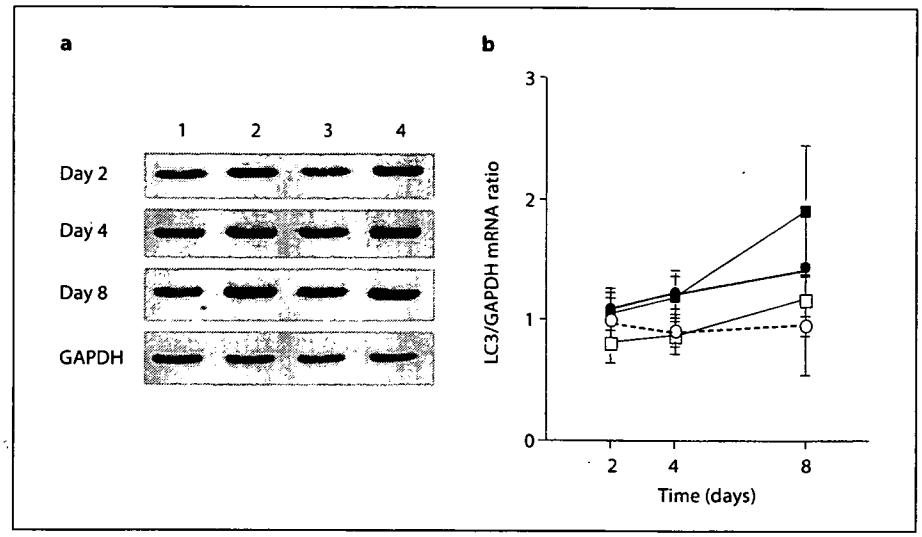

Fig. 3. a Semiquantitative analysis of relative LC3 mRNA levels in innervated (1, 3) and denervated soleus muscles (2, 4) from rats treated with saline (1, 2) and chloroquine (3, 4) on days 2, 4, and 8 based on RT-PCR. **b** Changes in LC3 mRNA levels in innervated (○, ●) and denervated rat soleus muscles (□, ■) on days 2, 4, and 8 of saline (○, □) or chloroquine treatment (●, ■). Values are normalized to the LC3 mRNA level in innervated muscles of saline-treated rats (control muscles). Means ± SD. n = 5 rats per group.

each band was quantified with NIH image (version 1.61) on a Macintosh computer. LC3, Apg5, Apg12, and GNE mRNA levels were normalized relative to GAPDH mRNA levels.

Statistical Analysis

Differences between control specimens and disease specimens were evaluated with a two-way analysis of variance. Multiple comparisons were made using Tukey's honestly significant difference test. A p value <0.05 was considered statistically significant.

Results

Histologic Study

Histologic findings for the innervated and denervated soleus muscles from saline- and chloroquine-treated rats on each test day were similar to those previously reported [2, 19] (fig. 1). Marked accumulation of dense granular bodies and vacuoles was present in chloroquine-treated muscles after denervation, particularly on day 8. By contrast, accumulation was not noted in the contralateral, innervated chloroquine-treated muscles or in the innervated and denervated muscles of the saline-treated rats. Quantitative analysis at the light-microscopic level showed that the fibers with dense granular bodies or vacuoles were present in innervated and denervated muscles from rats after chloroquine treatment (1.7 ± 1.2 and 12.8 ± 8.2% on day 2, 9.9 ± 1.7 and 20.4 ± 5.2% on day 4, and 9.9 ± 4.5 and 52.2 ± 15.0% on day 8, respectively). Further, fiber numbers were significantly greater in the denervated muscles than in the contralateral, innervated muscles (on day 4, $p = 0.0006$; on day 8, $p < 0.0001$). A few fibers with these bodies or vacuoles were found in the innervated and denervated muscles from saline-treated rats.

LC3 staining was minimal in innervated muscles from saline- and chloroquine-treated rats at all time points, whereas denervated muscles from both groups showed progressively stronger LC3 staining with increasing time (fig. 2). Strong positive reaction for LC3 was observed in the cytoplasm of muscle fibers, especially in the denervated muscles of chloroquine-treated rats.

Semiquantitative RT-PCR

To test for possible contamination of chromosomal DNA during RNA extraction, PCR amplification was performed without reverse transcription using the extracted RNA as a template. No bands appeared following 28 or 35 cycles of PCR, indicating the absence of contaminating DNA.

In the present study, LC3, Apg12 and Apg5 mRNA levels were measured in the innervated and denervated soleus muscles of saline- and chloroquine-treated rats on 2–8 days after initial injection of chloroquine (fig. 3–5). Experiments revealed that LC3, Apg5, and Apg12 were constitutively expressed in those muscles.

Significant changes in LC3 mRNA levels occurred as early as day 2 in the denervated muscles from chloroquine-treated rats (fig. 3). Further, mRNA levels were increased in these muscles on all test days when compared with the innervated muscles from saline-treated rats (control muscles), with the respective levels on days 2, 4 and 8 being 1.4, 1.6 and 1.8 times the control muscle levels, respectively. LC3 mRNA levels were significantly increased on days 4 and 8 in the denervated muscle of

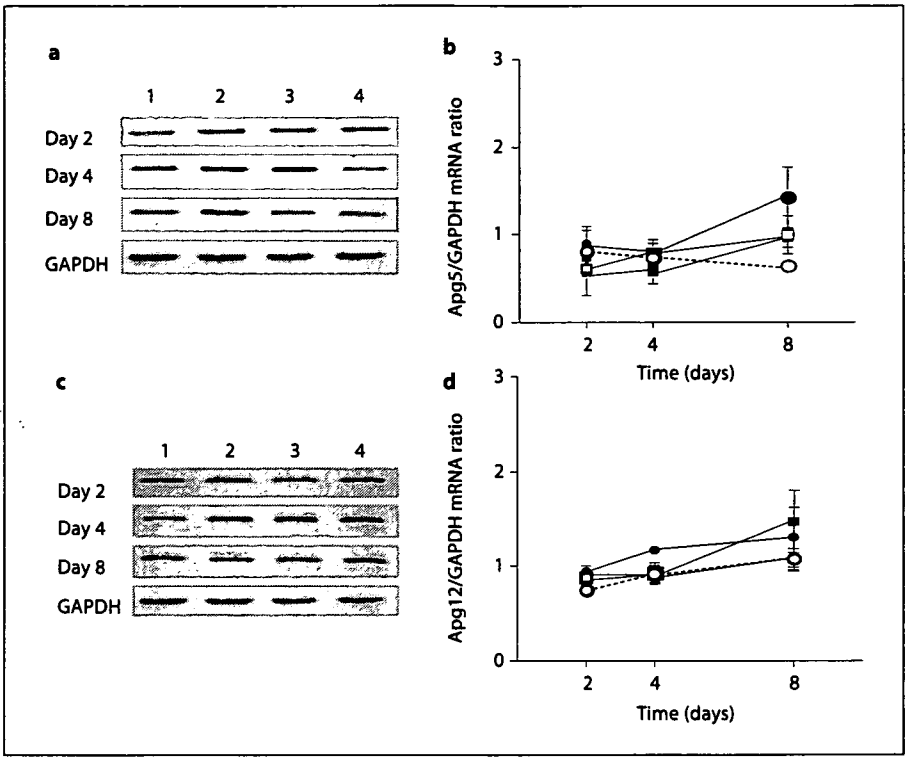

Fig. 4. a, c Semiquantitative analysis of relative Apg5 (**a**) and Apg12 (**c**) mRNA levels in innervated (1, 3) and denervated soleus muscles (2, 4) from saline (1, 2)- and chloroquine-treated rats (3, 4) on days 2, 4, and 8 based on RT-PCR. **b, d** Changes in Apg5 (**b**) and Apg12 (**d**) mRNA levels in innervated (○, ●) and denervated rat soleus muscles (□, ■) on days 2, 4, and 8 of saline (○, □) or chloroquine treatment (●, ■). Values are normalized to the Apg5 and Apg12 mRNA levels in innervated muscles of saline-treated rats (control muscles). Means ± SD. n = 5 rats per group.

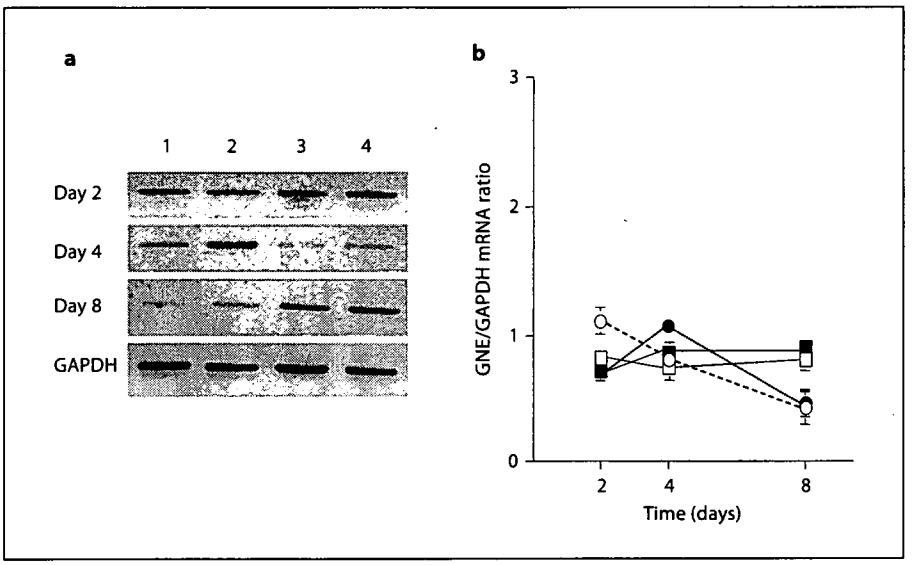

Fig. 5. a Semiquantitative analysis of relative GNE mRNA levels in innervated (1, 3) and denervated soleus muscles (2, 4) from saline (1, 2)- and chloroquine-treated rats (3, 4) on days 2, 4, and 8 based on RT-PCR. **b** Changes in GNE mRNA levels in innervated (○, ●)and denervated rat soleus muscles (□, ■) on days 2, 4, and 8 of saline (○, □) or chloroquine treatment (●, ■). Values are normalized to the GNE mRNA level in innervated muscles of saline-treated rats (control muscles). Means ± SD. n = 5 rats per group.

chloroquine-treated rats relative to those of the controls (on day 4, p = 0.051; on day 8, p = 0.001), but differences in mRNA levels on day 2 did not reach the levels of statistical significance. In the denervated muscles from saline-treated rats, LC3 mRNA levels progressively increased and were 1.1, 1.2 and 1.6 times those of control muscles, but the difference was not statistically significant. LC3 mRNA levels were increased in the denervated muscles from chloroquine-treated rats as compared with the levels from the denervated muscles from saline-treated rats, but this difference was not statistically significant.

Apg5 and Apg12 mRNA levels in the denervated muscles from saline-treated rats were 0.9-, 1.1-, and 1.4-, and 1.1-, 1.1-, and 1.3-fold those of the control on days 2, 4, and 8, whereas those in the denervated muscle from chlo-

roquine-treated rats were 0.8-, 0.8-, and 1.4-, and 1.1-, 1.2-, and 1.8-fold (fig. 4). However, no significant differences were found in the mRNA levels of Apg5 and Apg12 when comparing between the denervated muscles of both groups on each test day.

GNE was constitutively expressed in the innervated and denervated muscles from saline- and chloroquine-treated rats (fig. 5). GNE mRNA expression tended to decrease in association with chloroquine treatment but not with denervation. Further, mRNA levels tended to increase in denervated, chloroquine-treated muscles during the experiment, but there was no statistically significant difference in mRNA levels in those muscles relative to the control muscles and denervated, saline-treated muscles.

Discussion

Previous studies have reported marked and early accumulation of rimmed vacuoles consisting of dense granular bodies and variously sized vacuoles in the denervated muscles of chloroquine-treated rats [1–3]. By contrast, these vacuoles were very rare in the contralateral, innervated chloroquine-treated muscles as well as in the innervated and denervated muscles of saline-treated rats. We previously reported significant increases in lysosomal enzyme (cathepsins B and L) activity and lysosome-related transport proteins, such as clathrin protein, and mRNA levels and mannose-6-phosphate receptor (M6PR) mRNA levels in the denervated muscles of chloroquine-treated rats compared with that in the innervated muscles of saline-treated rats [1, 2, 19, 20]. These data suggest that the autophagic-lysosome system, especially generation of early endosomes, is increased, as manifested by the formation of lysosomal enzyme-containing clathrin-coated vesicles from the trans-Golgi network of the Golgi apparatus (an endosomal pathway) [1, 2, 19, 20]. However, the autophagic process in these muscles has not yet been studied.

Both Apg5 and Apg12 are located only in the pre-autophagosomal structure (PAS), which precedes isolated membrane formation, and in the autophagosomal precursor but not in autophagosomes or autolysosomes [7, 13, 21, 22]. LC3 is present mainly in autophagosomes and some autolysosomes as well as the autophagosomal precursor [13, 22]. Autophagy is induced under various conditions. After breakdown of muscle fibers, segregation of cytoplasmic materials (e.g. proteins and lipids) and organelles (e.g. mitochondria and cell membranes) are surrounded with the membrane of autophagosomal precursor, and then autophagosomes are formed. The fusion of the outer membrane of autophagosomes with the membrane of early endosomes containing lysosomal enzymes then leads to the formation of autolysosomes [22]. In autolysosomes, segregated cytoplasmic materials or organelles are degraded by lysosomal enzymes, such as cathepsins B and L [2, 4]. Although PAS is present in yeast [22], it is not clear whether PAS is present in animal cells.

In the present study, we measured mRNA levels of Apg12, Apg5 and LC3 in innervated and denervated muscles from saline- and chloroquine-treated rats and demonstrated expression of these genes in all experimental muscles. This suggests that the Apg12-conjugated Apg5 and LC3 systems may play an important role in physiological and pathological conditions in rat muscles. Previous reports have indicated that the Apg12-conjugated Apg5 system may be involved in autophagosome formation and completion in mammalian cells as well as in yeast cells [6, 7, 21]. However, the present study demonstrated that Apg12 and Apg5 mRNA levels were not significantly increased in denervated muscles of chloroquine-treated muscles, which have numerous dense granular bodies and vacuoles consisting mainly of autophagosomes compared with contralateral innervated muscles and with denervated and innervated muscles from saline-treated muscles.

The present study demonstrated that LC3 mRNA levels were increased in denervated muscles of chloroquine-treated rats relative to those in denervated muscles of saline-treated rats or innervated muscles of both rat groups from days 2–8. An increase in the formation of rimmed vacuoles containing dense granular bodies and vacuoles in denervated muscles of chloroquine-treated rats was observed as early as day 2, with progressive increases thereafter. Further, the number of muscle fibers with these bodies and vacuoles increased along with the elevation of LC3 mRNA levels. These results suggest that LC3 may regulate autophagy and autophagosome formation in skeletal muscle and is consistent with previous in vitro data [9, 12, 13, 21]. Therefore, chloroquine may induce autophagosome formation in the skeletal muscle without inhibiting LC3 expression.

In the present study, LC3 protein and mRNA levels significantly increased exclusively in denervated muscles from chloroquine-treated rats, whereas the mRNA levels of Apg12 and Apg5 did not change significantly. This discrepancy seems to be due to the fact that changes in Apg12 and Apg5 mRNA levels are small. Further, it may be difficult to detect changes in Apg12 and Apg5 mRNA levels if the rate of turnover from PAS and the autophagosomal precursor to the autophagosome is very rapid. However,

the nature of the interaction between the Apg12-Apg5 conjugate and LC3 at the transcriptional and molecular levels remains unclear.

The present and previous studies showed that mRNA or protein levels of major lysosome-related proteins, such as M6PR, clathrin, α- and γ-adaptins, Golgi-zone protein and LC3, were increased in the denervated muscles from chloroquine-treated rats that had numerous muscle fibers with rimmed vacuoles [19, 20]. This suggests that the lysosome system, especially the transport of newly synthesized lysosomal enzymes from the secretory pathway via the trans-Golgi network and autophagosome formation, is activated in these muscles. However, the etiology and the pathomechanism of abnormal accumulation of rimmed vacuoles remain unclear. Recently, a GNE gene mutation has been detected in cases of familial inclusion body myopathy and distal myopathy with rimmed vacuoles [14, 15] associated with accumulation of rimmed vacuoles containing autophagosomes and autolysosomes, suggesting that a certain lysosome system abnormality may be responsible for rimmed vacuole formation. Although the expression of GNE in chloroquine-induced myopathy has not been studied previously, the present study demonstrated expression of GNE in innervated and denervated muscles from chloroquine- and saline-treated rats. However, skeletal muscle GNE mRNA levels did not change significantly after chloroquine or denervation treatments compared with control muscles. Thus, the role of GNE in the rimmed vacuole formation remains unclear.

In the present study, LC3 mRNA levels increased in association with rimmed vacuole formation in chloroquine-induced myopathy, suggesting an increase in autophagy at the molecular level. However, because of the expression of GNE, which may mediate formation of rimmed vacuoles in human skeletal muscles, we speculate that abnormal accumulation of rimmed vacuoles consisting of autophagosomes and autolysosomes in denervated muscles from chloroquine-treated rats may be due to slow turnover of autolysosomal degradation process at or after the fusion of early endosomes with autophagosomes. However, this process does not appear to be meditated by abnormalities in the early endosome or in autophagosome-related genes or proteins.

Acknowledgments

We are grateful to Ms. Y. Umeki, Ms. M. Ono, and Ms. K. Hirano for their technical assistance.

References

1 Kumamoto T, Araki S, Watanabe S, Ikebe N, Fukuhara N: Experimental chloroquine myopathy: morphological and biochemical studies. Eur Neurol 1989;29:202–207.
2 Kumamoto T, Ueyama H, Watanabe S, Murakami T, Araki S: Effect of denervation on overdevelopment of chloroquine-induced autophagic vacuoles in skeletal muscles. Muscle Nerve 1993;16:819–826.
3 Stauber WT, Hedge AM, Trout JJ, Schottelius BA: Inhibition of lysosomal function in red and white skeletal muscles by chloroquine. Exp Neurol 1981;71:295–306.
4 Bird JWC: Skeletal muscle lysosomes; in Dingle JT, Dean RT (eds): Lysosomes in Biology and Pathology. Amsterdam, North-Holland, 1975, vol 4, pp 75–109.
5 Gerard KW, Hipkiss AR, Schneider DL: Degradation of intracellular protein in muscle. Lysosomal response to modified proteins and chloroquine. J Biol Chem 1988;263:18886–18890.
6 Mizushima N, Noda T, Ohsumi Y: Apg16p is required for the function of the Apg12p-Apg5p conjugate in the yeast autophagy pathway. EMBO J 1999;18:3888–3896.
7 Mizushima N, Yamamoto A, Hatano M, Kobayashi Y, Kabeya Y, Suzuki K, Tokuhisa T, Ohsumi Y, Yoshimori T: Dissection of autophagosome formation using Apg5-deficient mouse embryonic stem cells. J Cell Biol 2001;152:657–668.
8 Ichimura Y, Kirisako T, Takao T, Satomi Y, Shimonishi Y, Ishihara N, Mizushima N, Tanida I, Kominami E, Ohsumi M, Noda T, Ohsumi Y: A ubiquitin-like system mediates protein lipidation. Nature 2000;408:488–492.
9 Nemoto T, Tanida I, Tanida-Miyake E, Minematsu-Ikeguchi N, Yokota M, Ohsumi M, Ueno T, Kominami E: The mouse APG10 homologue, an E2-like enzyme for Apg12p conjugation, facilitates MAP-LC3 modification. J Biol Chem 2003;278:39517–39526.
10 Ohsumi Y: Molecular dissection of autophagy: two ubiquitin-like systems. Nat Rev Mol Cell Biol 2001;2:211–216.
11 Tanida I, Sou YS, Ezaki J, Minematsu-Ikeguchi N, Ueno T, Kominami E: HsAtg4B/HsApg4B/autophagin-1 cleaves the carboxyl termini of three human Atg8 homologues and delipidates microtubule-associated protein light chain 3- and GABAA receptor-associated protein-phospholipid conjugates. J Biol Chem 2004;279:36268–36276.
12 Kirisako T, Ichimura Y, Okada H, Kabeya Y, Mizushima N, Yoshimori T, Ohsumi M, Takao T, Noda T, Ohsumi Y: The reversible modification regulates the membrane-binding state of Apg8/Aut7 essential for autophagy and the cytoplasm to vacuole targeting pathway. J Cell Biol 2000;151:263–276.
13 Kabeya Y, Mizushima N, Ueno T, Yamamoto A, Kirisako T, Noda T, Kominami E, Ohsumi Y, Yoshimori T: LC3, a mammalian homologue of yeast Apg8p, is localized in autophagosome membranes after processing. EMBO J 2000;19:5720–5728.
14 Arai A, Tanaka K, Ikeuchi T, Igarashi S, Kobayashi H, Asaka T, Date H, Saito M, Tanaka H, Kawasaki S, Uyama E, Mizusawa H, Fukuhara N, Tsuji S: A novel mutation in the GNE gene and a linkage disequilibrium in Japanese pedigrees. Ann Neurol 2002;52:516–529.

15 Eisenberg I, Avidan N, Potikha T, Hochner H, Chen M, Olender T, Barash M, Shemesh M, Sadeh M, Grabov-Nardini G, Shmilevich I, Friedmann A, Karpati G, Bradley WG, Baumbach L, Lancet D, Asher EB, Beckmann JS, Argov Z, Mitrani-Rosenbaum S: The UDP-N-acetylglucosamine 2-epimerase/N-acetylmannosamine kinase gene is mutated in recessive hereditary inclusion body myopathy. Nat Genet 2001;29:83–87.
16 Zhou B, Boudreau N, Coulber C, Hammarback J, Rabinovitch M: Microtubule-associated protein 1 light chain 3 is a fibronectin mRNA-binding protein linked to mRNA translation in lamb vascular smooth muscle cells. J Clin Invest 1997;100:3070–3082.
17 Stasche R, Hinderlich S, Weise C, Effertz K, Lucka L, Moormann P, Reutter W: A bifunctional enzyme catalyzes the first two steps in N-acetylneuraminic acid biosynthesis of rat liver. Molecular cloning and functional expression of UDP-N-acetyl-glucosamine 2-epimerase/N-acetylmannosamine kinase. J Biol Chem 1997;272:24319–24324.
18 Tso JY, Sun XH, Kao TH, Reece KS, Wu R: Isolation and characterization of rat and human glyceraldehyde-3-phosphatedehydrogenase cDNAs: genomic complexity and molecular evolution of the gene. Nucleic Acids Res 1985;13:2485–2502.
19 Masuda T, Ueyama H, Nakamura K, Jikumaru M, Toyoshima I, Kumamoto T: Skeletal muscle expression of clathrin and mannose 6-phosphate receptor in experimental chloroquine-induced myopathy. Muscle Nerve 2005;31:495–502.
20 Kumamoto T, Nagao SI, Sugihara R, Abe T, Ueyama H, Tsuda T: Effect of chloroquine-induced myopathy on rat soleus muscle sarcoplasm and expression of clathrin. Muscle Nerve 1998;21:665–668.
21 Mizushima N, Yamamoto A, Matsui M, Yoshimori T, Ohsumi Y: In vivo analysis of autophagy in response to nutrient starvation using transgenic mice expressing a fluorescent autophagosome marker. Mol Biol Cell 2004;15:1101–1111.
22 Suzuki K, Kirisako T, Kamada Y, Mizushima N, Noda T, Ohsumi Y: The pre-autophagosomal structure organized by concerted functions of APG genes is essential for autophagosome formation. EMBO J 2001;20:5971–5981.

Neuropathology 2007; **27**, 522–530 doi:10.1111/j.1440-1789.2007.00822.x

Original Article

Role of proteasomes in the formation of neurofilamentous inclusions in spinal motor neurons of aluminum-treated rabbits

Noriyuki Kimura,[1] Toshihide Kumamoto,[1] Hidetsugu Ueyama,[1] Hideo Horinouchi[1] and Eisaku Ohama[2]

[1]Department of Neurology and Neuromuscular Disorders, Oita University, Faculty of Medicine, Oita, and [2]Department of Neuropathology, Institute of Neurological Sciences, Faculty of Medicine, Tottori University, Yonago, Japan

We examined the role of the 20S proteasome in pathologic changes, including abnormal aggregation of phosphorylated neurofilaments, of spinal motor nerve cells from aluminum-treated rabbits. Immunohistochemistry for the 20S proteasome revealed that many lumbar spinal motor neurons without intracytoplasmic neurofilamentous inclusions or with small inclusions were more intensely stained in aluminum-treated rabbits than in controls, whereas the immunoreactivity was greatly decreased in some enlarged neurons containing large neurofilamentous inclusions. Proteasome activity in whole spinal cord extracts was significantly increased in aluminum-treated rabbits compared with controls. Furthermore, Western blot analysis indicated that the 20S proteasome degraded non-phosphorylated high molecular weight neurofilament (neurofilament-H) protein *in vitro*. These results suggest that aluminum does not inhibit 20S proteasome activity, and the 20S proteasome degrades neurofilament-H protein. We propose that abnormal aggregation of phosphorylated neurofilaments is induced directly by aluminum, and is not induced by the proteasome inhibition in the aluminum-treated rabbits. Proteasome activation might be involved in intracellular proteolysis, especially in the earlier stages of motor neuron degeneration in aluminum-treated rabbits.

Key words: aluminum intoxication, neurofilament degradation, neurofilamentous inclusion, proteasome, spinal motor neuron.

Correspondence: Noriyuki Kimura, MD, Department of Neurology and Neuromuscular Disorders, Oita University, Faculty of Medicine, Idaigaoka 1-1, Hasama, Yufu, Oita 879-5593, Japan. Email: noriyuki@med.oita-u.ac.jp

Received 1 November 2006; revised 16 March 2007 and accepted 17 March 2007.

INTRODUCTION

Neurofilamentous inclusions representing the intraneuronal accumulation of phosphorylated neurofilament protein are observed in some neurodegenerative diseases, most notably in the spinal motor neurons of amyotrophic lateral sclerosis (ALS).[1,2] To examine this pathologic change, acute and chronic aluminum neurotoxicity has been studied exclusively in New Zealand white rabbits using intravenous,[3] intracisternal,[4–7] intracerebral,[8–10] and oral routes[11] of administration. Although the severity of the neurologic and neuropathologic changes varies with the dosage and duration of aluminum administration, the neuropathologic hallmark of aluminum neurotoxicity is the accumulation of phosphorylated neurofilament protein in the neuronal cytoplasm, dendrites, and axons throughout the central nervous system.[3,5,7,8,11,12] Spinal motor neurons are particularly sensitive to aluminum neurotoxicity.[13] Therefore, acute or chronic aluminum intoxication is an appropriate model to study the formation of neurofilamentous inclusions in spinal motor neurons. The mechanism of aluminum-induced accumulation of phosphorylated neurofilament protein is unknown, but the evidence suggests that aluminum inhibits axonal transport,[14] dephosphorylation of neurofilament protein,[5] and incorporation of neurofilament subunits synthesized de novo into the cytoskeleton.[15] In addition, it has also been reported that aluminum inhibits the degradation of neurofilament protein by intracellular proteases such as calcium-dependent (i.e., calpain) and -independent (i.e., lysosomal cathepsins) proteases.[16,17]

Proteasomes are essential enzymes in the ubiquitin-dependent and -independent non-lysosomal proteolytic system and, in addition to calpain and cathepsins, are involved in the majority of intracellular proteolysis.[18–20]

Recent studies demonstrated that dysfunction of the ubiquitin-proteasome system is related to various neurodegenerative disorders, including ALS.[21-23] In aluminum-treated rabbits, proteasomes might also be involved in the formation of neurofilamentous inclusions, because the cytoplasm of spinal motor neurons with these inclusions is strongly immunoreactive for ubiquitin.[7] However, the role of proteasomes is not known in the pathologic changes of the spinal motor neurons after aluminum treatment. To clarify the role of the 20S proteasome, the proteolytic core of the proteasome, in the formation of neurofilamentous inclusions, we examined its expression and activity in the aluminum-intoxicated rabbits. Furthermore, we examined whether neurofilament-H protein is degraded by the 20S proteasome *in vitro*.

METHODS

Animals

Ten male adult New Zealand white rabbits (9 weeks old) were obtained from Seac Yoshitomi (Fukuoka, Japan). Animals were housed at the Oita University Animal Care Center and given access to water and food pellets. All experiments conformed to the Guidelines for Animal Experiments of Oita University Faculty of Medicine. In all rabbits, a small craniotomy was made in the anterior portion of the left side of the cranium with a dental drill under ether anesthesia. Animals were injected through the craniotomy into the dorsal parietal region with 0.5 mL of Holt adjuvant (5.6 mL 10% $AlCl_3$·E6 H_2O, 27.9 mL distilled water, 6.3 mL 15.75% Na_3PO_4·E12H_2O, pH 5.5, $n = 5$) or phosphate-buffered saline (PBS, pH 5.5, $n = 5$), as previously reported.[8-10] For the proteasome activity assay, all control and aluminum-treated rabbits were first perfused with physiologic saline on day 7 after the initial injections, according to previous reports.[24-26] The lumbar spinal cord was removed from each animal and then rapidly frozen in liquid nitrogen. The specimens were stored at –80°C until use. The rabbits were perfused again with buffered 4% formalin for histological studies. After perfusion, the cervical, thoracic, and lumbar segments of each spinal cord were immersion-fixed in 10% formalin (pH 7.0) at room temperature for 48 h.

Clinical examination

After aluminum administration, each rabbit was weighed and evaluated daily for spontaneous behavior, posture, reaction to handling and gait.

Histological and immunohistochemical studies

After fixation in 10% formalin, spinal cords were embedded in paraffin, and then consecutive 6-μm thick transverse sections were cut on a microtome. The sections were stained with HE and by the modified Bielschowsky method.[27]

For immunohistochemical analysis, sections were deparaffinized in xylene, rehydrated in a graded ethanol series, and then equilibrated in 10 mM PBS (pH 7.4). Sections were incubated for 30 min in PBS containing 10% (w/v) non-fat dry milk, then overnight with a mouse monoclonal antibody against phosphorylated neurofilament-H protein (SMI 31, diluted 1:1000, Sternberger Monoclonals, Baltimore, MD, US) in a moist chamber at 4°C. After washing with PBS, the sections were incubated with biotinylated goat antimouse IgG (diluted 1:100, Vector Laboratories, Burlingame, CA, US) for 1 h, and then for 30 min at room temperature using a Vectastain ABC Elite Kit (Vector Laboratories). Antibody binding sites were made visible by staining with 0.02% 3, 3′-diaminobenzidine tetrahydrochloride plus 0.01% H_2O_2 for 10 min. The sections were counterstained with hematoxylin.

For two-color immunofluorescence analysis, the sections were incubated overnight with a polyclonal rabbit antibody against the 20S proteasome (diluted 1:200, Biomol International, Plymouth Meeting, PA, US) and SMI 31 at 4°C, then fluorescein isothiocyanate (FITC)-labeled horse antirabbit IgG (diluted 1:100, Vector Laboratories) and rhodamine-labeled donkey antimouse IgG (diluted 1:100, Chemicon International, Temecula, CA, US) for 60 min, respectively. Using a Carl Zeiss LSM5 Pascal-V3.2 confocal microscopy system (Carl Zeiss, Jena, Germany), the cells that were strongly positive for the 20S proteasome or SMI 31 were counted and reported as a percentage of at least 100 spinal motor neurons in each specimen.

The intensity of immunostaining for the proteasome antibody was classified into three groups: (–), weaker than control level; (+), equivalent to control level; and (++), greater than control level. Intensity was determined on color prints of fluorescence micrographs of each specimen in a blind manner. The number of proteasome-positive neurons was counted in 100 motor nerve cells in the lumbar spinal cord from each aluminum-treated rabbit three times.

The size of the intracytoplasmic neurofilamentous inclusions was expressed as the percentage of area stained strongly positive for SMI 31 occupying the cytoplasm of each motor neuron. The areas of SMI 31 positive inclusions and 20S proteasome positive cytoplasmic regions were measured for 20 motor nerve cells from each spinal cord specimens of aluminum-treated rabbit using an Image J software (Rasband, W.S., Image J, US National Institutes of Health, Bethesda, MD, US).

The immunostaining was specific as determined by the absence of staining when sections were incubated without

the primary antibodies or when normal mouse serum and normal rabbit serum were substituted for the primary antibodies.

Proteasome activity

Lumbar spinal cords (1–1.2 g) from the controls ($n = 5$) and the aluminum-treated rabbits ($n = 5$) were sonicated in 10 volumes of ice-cold 50 mM Tris-HCl (pH 7.5) containing 1 mM EDTA, using an ultrasonic tissue disrupter at power level 4 (Ultra Heat System Inc. New York, NY, US). Proteasome activity in the spinal cord extracts was assayed using Suc-Leu-Leu-Val-Try-4-methyl-coumaryl-7-amide (MCA, Peptide Institute, Minoh, Osaka, Japan). In brief, the reaction mixture (1 mL) containing 50 mM Tris-HCl (pH 7.5), 1 mM EDTA, 65 μM Suc-Leu-Leu-Val-Try-MCA, and 100 μL of sample was incubated at 25°C for 60 min. The activity was determined by measuring the generation of MCA, the fluorogenic cleavage product, at 390 and 465 nm (excitation and emission, respectively) with a XFLUOR4 (Wako Pure Chemical Industries, Tokyo, Japan). Enzyme activity was defined as fluorescence units (FU) per minute per microgram protein. The specificity of the proteasome assay was confirmed by incubation with 10 μM lactacystin, a proteasome inhibitor (Affinity Research Products, Mamhead Castle, Mamhead, UK), which almost completely inhibited the fluorescence change. The protein concentration was measured using the method of Lowry *et al.*[28]

Assay of neurofilament-H protein degradation by the 20S proteasome

One microgram of bovine neurofilament-H protein (Affinity Research Products) was incubated in 100 μL of reaction mixture. The reaction mixture contained 50 mM Tris-HCl, pH 7.5, 0.02% Tween 20, and various concentrations (0, 6.25, 50, and 100 nM) of bovine 20S proteasome (Affinity Research Products). Reaction mixtures were incubated at 37°C for 0–6 h. Samples (200 ng of protein) were resolved by electrophoresis in 5% sodium dodecyl sulfate-polyacrylamide gel electrophoresis as described by Laemmli.[29] The gels were transferred onto nitrocellulose membranes (Amersham Pharmacia Biotech, Little Chalfont Buckinghamshire, UK) and incubated overnight with a mouse monoclonal antibody against neurofilament-H protein (N52, diluted 1:2000, Sigma Chemical, St. Louis, MO, US) at 4°C and then for 60 min with peroxidase-conjugated sheep antimouse IgG antibody (Amersham Pharmacia Biotech, diluted 1:5000 with PBS). Stained protein bands were observed with enhanced chemiluminescence (Amersham Pharmacia Biotech) and scanned using the transparent mode of the scanner into a Macintosh computer. Data in relative units were analyzed using Image J.

Data analysis

Data were expressed as mean values ± SD and statistically analyzed using the unpaired *t*-test. Relationships between variables were evaluated by linear regression analysis. A *P*-value of <0.05 was considered statistically significant.

RESULTS

Clinical findings

The body weight of all control rabbits increased during the experiment, whereas that of a large number of aluminum-treated rabbits slightly decreased, but some did not change. The mean body weights of the controls and aluminum-treated rabbits were, respectively, 2.32 kg ± 0.07 and 2.20 kg ± 0.09 before aluminum administration, and 2.44 kg ± 0.11 and 2.24 kg ± 0.1 1 week after the initial administration. There were no significant changes in mean body weight before or after the exposure to aluminum. Aluminum-treated rabbits tended to have deceased movement due to hindleg weakness, and gait disturbance, particularly 7 days after the injection, whereas control rabbits had no muscle weakness.

Histologic and immunohistochemical findings

Spinal cords from control rabbits appeared normal macroscopically, but those from aluminum-treated rabbits occasionally softened and had a grayish coloration.

Histological examination of the spinal cords from the control rabbits revealed a normal morphology: the cytoplasm of the spinal motor neurons was not argentophilic, but numerous argentophilic axons were observed using a modified Bielschowsky stain (Fig. 1a). In contrast, the spinal motor neurons from aluminum-treated rabbits contained numerous neurofilamentous inclusions in their cytoplasm, appearing argentophilic with a modified Bielschowsky stain (Fig. 1b). Most neurofilamentous inclusions were small and occupied only a limited portion of the cytoplasm, while some large inclusions extended from the cytoplasm into the neurites. There were also argentophilic axonal spheroids or globules. The number of normal argentophilic axons was decreased in the anterior horn (Fig. 1b). These findings were also observed in the cervical and thoracic segments, but were more prominent in the lumbar segments.

Immunostaining for SMI 31 was negative in the cytoplasm and neurites of the spinal motor neurons from control rabbits (Fig. 1c). In the aluminum-treated rabbits, strong immunoreactivity for SMI 31 was observed in the cytoplasm and neurites of spinal motor neurons. Numerous small or large neurofilamentous inclusions were intensely immunostained with SMI 31 (Fig. 1d). The small sized SMI

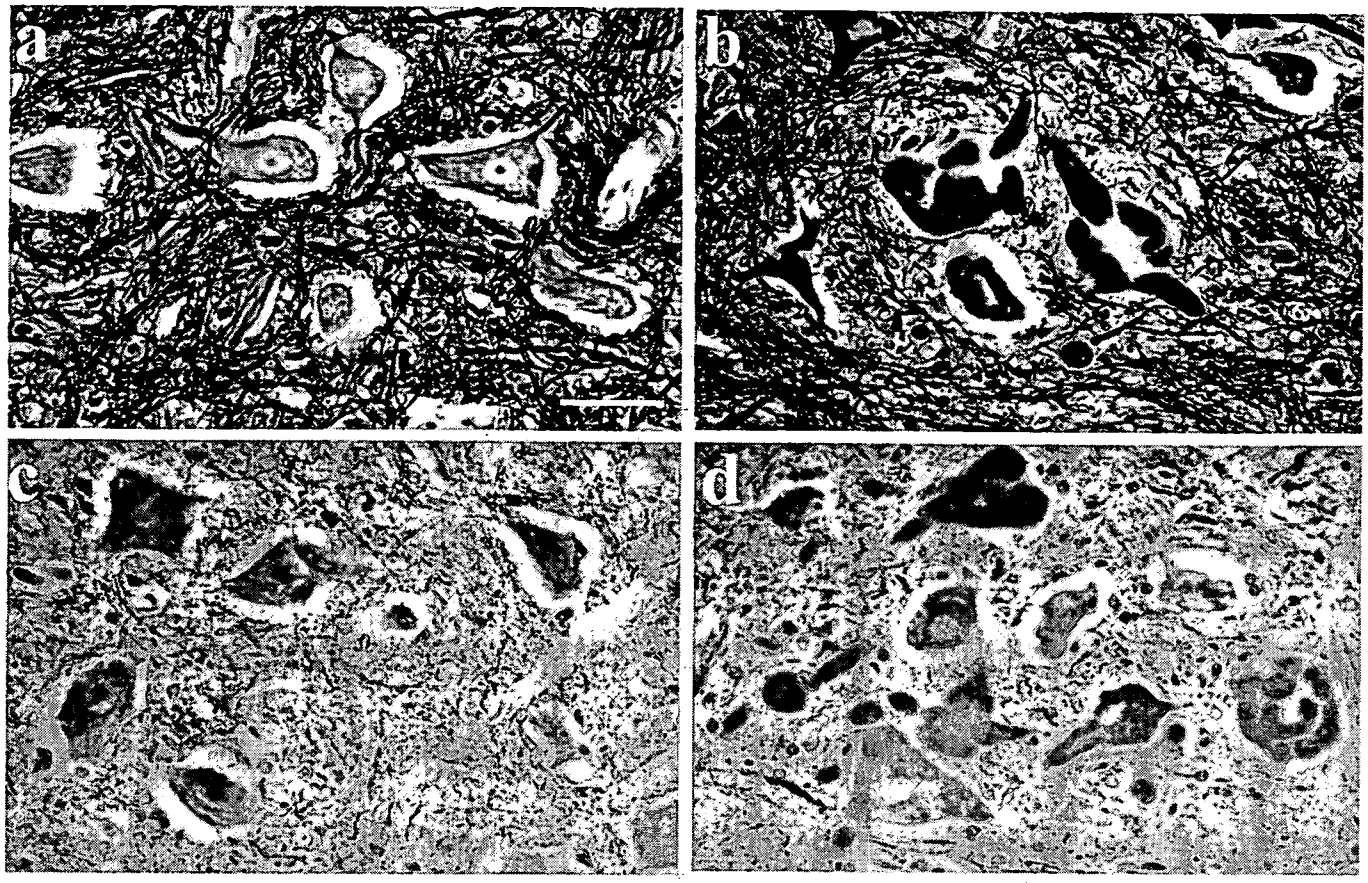

Fig. 1 Anterior horn of the lumbar spinal segments from control (a, c) and aluminum-treated (b, d) rabbits. Aluminum-treated motor neurons contain argentophilic filamentous inclusions (b), which are immunostained with antiphosphorylated neurofilament-H protein antibody (SMI 31) in the cytoplasm, dendrites and proximal axons (d). (a, b) modified Bielschowski stain; (c, d) immunostaining with SMI 31. Bar =*50* μm.

31 positive inclusions were exclusively located in the peripheral cytoplasmic region of motor neurons. The axonal spheroids and globules were also intensely immunostained.

The cytoplasm, dendrites, and sometimes nucleus of the spinal motor neurons from control rabbits exhibited only a faint immunohistochemical reaction to the 20S proteasome, but were negative for SMI 31 (Fig. 2a–c). In the aluminum-treated rabbits, immunostaining for 20S proteasomes also showed positive reaction in the cytoplasm of spinal motor neurons with and without these small SMI 31 positive inclusions (Fig. 2d–f), while it was decreased in the enlarged neurons containing large SMI 31 positive inclusions (Fig. 2g–i). Various sized SMI 31 positive inclusions, representing phosphorylated neurofilaments, and axonal spheroids or granules were negative for 20S proteasomes. The immunoreactivity for 20S proteasome and SMI 31 did not co localize in the cytoplasm, dendrites, or nucleus.

The intensity of 20S proteasome immunoreactivity in the cytoplasm of spinal motor neurons was classified into three groups: (–), weaker than control level; (+), equivalent to control level; and (++), greater than control level. The frequencies of 20S proteasome-positive motor neurons were 29.7% in the (–) group, 30.0% in the (+), and 40.3% in the (++), respectively. The percentage was significantly higher in the (++) group than in the (–) or (+) group (P = 0.0033 or 0.0042; Table 1). The ratio of area reacted strongly positive for SMI 31 in the cytoplasm was signifi-

Table 1 Comparison of the number of motor neurons between three degrees of proteasome immunoreactivity

Proteasome immunoreactivity		
Immunoreactivity	Motor neuron (n = 100)	P-value
(–)	29.7 ± 2.5	0.0033*
(+)	30.0 ± 2.6	0.0042*
(++)	40.3 ± 1.5	—

*P < 0.05. The intensity of immunoreactivity with the proteasome antibody was classified into three groups: (–), weaker than control level; (+), equivalent to control level; and (++), greater than control level. The frequencies of neurons of (++) group was significantly greater than that of the (–) and (+) groups. P-values versus (++) group are given.

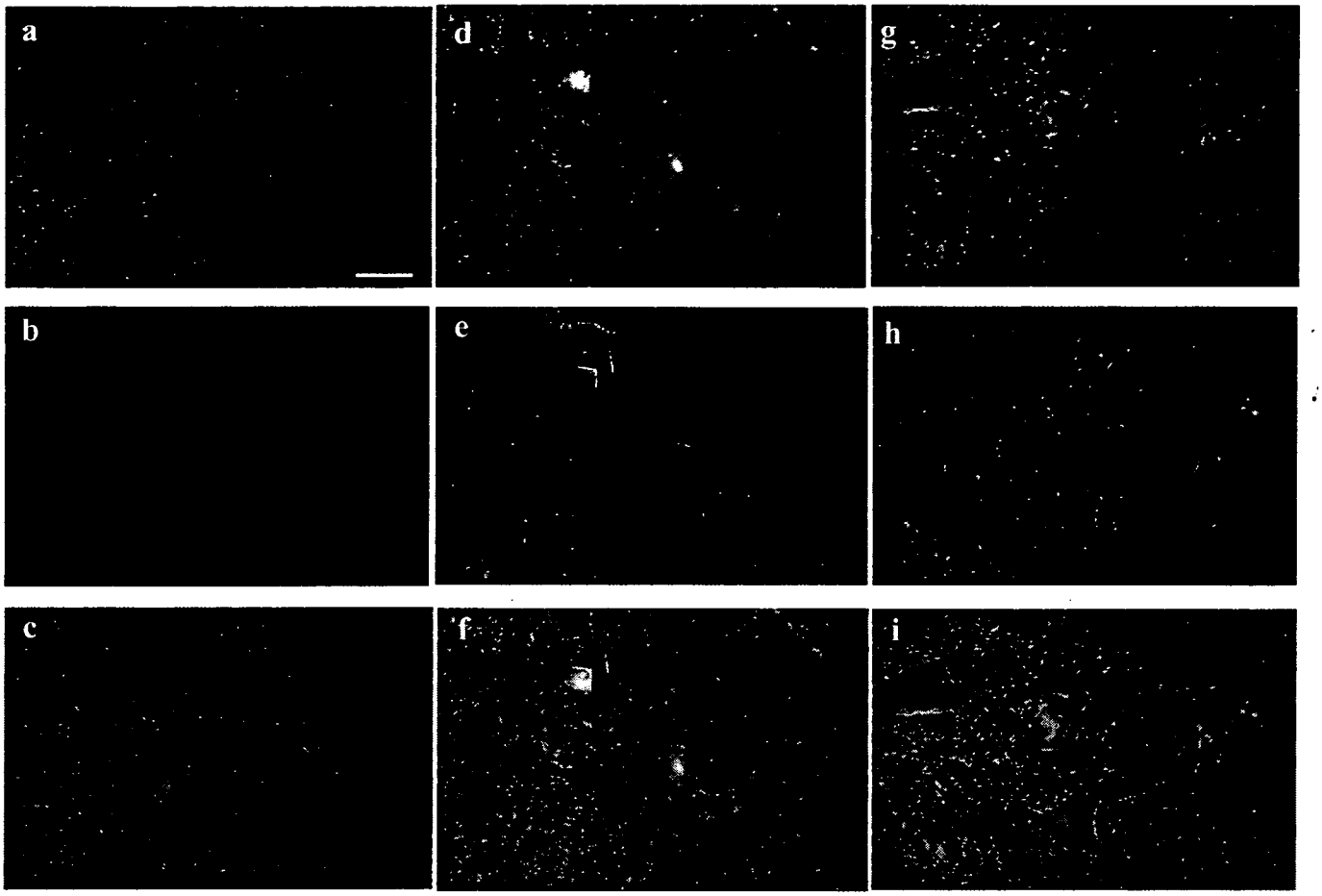

Fig. 2 Two-color immunofluorescence analyses with anti20S proteasome (green fluorescence) and SMI 31 (red fluorescence) antibody. In control rabbits, the cytoplasm and dendrites of the spinal motor neurons were faintly positive for the anti20S proteasome and negative for SMI 31 (a–c). In the aluminum-treated rabbits, the neurofilamentous inclusions were positive for SMI 31. Motor neurons with and without small-sized neurofilamentous inclusions had increased 20S proteasome immunoreactivity in the cytoplasm (d–f), while the enlarged neurons containing large-sized neurofilamentous inclusions had decreased immunoreactivity (g–i).Bar = 50 μm.

cantly larger in the (–) group than in the (+) or (++) group ($P < 0.0001$ and $P < 0.0001$) (Fig. 3).

Proteasome activity

Proteasome activity in the lumber spinal cord extracts from the control and aluminum-treated rabbits was 7.5 ± 0.2 FU/min/μg and 9.6 ± 0.2 FU/min/μg, respectively. The values were significantly greater in the aluminum-treated rabbits than in controls ($P < 0.0001$; Fig. 4).

Degradation of high molecular subunit neurofilament (neurofilament-H) protein by the 20S proteasome

The results of *in vitro* study of the degradation of neurofilament-H protein with and without the 20S proteasome are shown in Figure 5. Incubation of neurofilament-H protein without the 20S proteasome for 0–6 h did not yield any degradation products (Fig. 5a). The intensity of the band corresponding to the neurofilament-H protein clearly decreased when incubated with the 20S proteasome for 2–6 h and a 180-kDa band concomitantly appeared (Fig. 5b). After 6 h of incubation, neurofilament-H protein was degraded by approximately 57%. Degradation of neurofilament-H protein by the 20S proteasome was significantly inhibited by the addition of 10 μM lactacystin, a proteasome inhibitor (Fig. 5c). Degradation of neurofilament-H protein by the 20S proteasome closely correlated with the 20S proteasome concentration (0–100 nM) when incubated for 6 h ($P < 0.001$, $r = 0.998$; Fig. 6).

DISCUSSION

The abnormal intraneuronal accumulation of phosphorylated neurofilament-H protein, observed histologically as